Journal of Catalysis 263 (2009) 359–371

Contents lists available at ScienceDirect

Journal of Catalysis

www.elsevier.com/locate/jcat

A general method for determining the role of spectroscopically observed species in reaction mechanisms: Analysis of coverage transients (ACT)

Travis Gott, S. Ted Oyama *

Environmental Catalysis and Nanomaterials Laboratory, Department of Chemical Engineering, Virginia Tech, Blacksburg, VA 24061, USA

ARTICLE INFO

Article history:
Received 3 January 2009
Revised 20 February 2009
Accepted 23 February 2009
Available online 19 March 2009

Keywords:
Hydrodenitrogenation
Mechanism, transient coverage analysis
In situ FTIR
Pyridine
2,3,4,5-Tetrahydropyridine
Nickel phosphide

ABSTRACT

A kinetic method is described to determine the role of adsorbed intermediates in heterogeneous reaction mechanisms. The method, denoted as analysis of coverage transients (ACT), involves comparing the time response of a spectroscopically observed species in an inert gas and a reactive gas to differentiate between adsorption–desorption processes and reaction. The method is applied in a kinetic study of pyridine hydrodenitrogenation (HDN) on a 12.2 wt% silica-supported nickel phosphide (Ni_2P/SiO_2) catalyst at 423 K and atmospheric pressure. In situ Fourier transform infrared spectroscopy (FTIR) measurements of pyridine adsorbed on Ni_2P revealed the formation of a pyridinium surface intermediate. The concentration of the pyridinium intermediate increased with pyridine partial pressure and decreased in the presence of hydrogen, suggesting that it was a reaction intermediate. However, transient and steady-state kinetic measurements showed that the rate of reaction of the intermediate did not correspond to the overall reaction rate, and it is concluded that the pyridinium intermediate is not directly involved in the HDN reaction of pyridine over Ni_2P. The studies demonstrate that mere observation of an adsorbed surface species at reaction conditions is not sufficient to prove that it is a reaction intermediate. The ACT method has potential as it can be used with any type of spectroscopy, as long as the surface coverage can be calibrated.

1. Introduction

Directly monitoring the surface concentration of an adsorbed surface species during adsorption and reaction is a powerful tool for elucidating kinetic and mechanistic information [1]. Such studies involve measuring the rates of adsorption and reaction under transient conditions and comparing the transient rates with the overall reaction rate measured under steady-state conditions [2,3]. Agreement between the separately measured rates constitutes proof that the observed intermediate is a true reaction intermediate and is kinetically significant in the overall reaction kinetics. The present study will present a method, called analysis of coverage transients (ACT) to show that a species observed in situ spectroscopically, although responding to reaction conditions, is not an actual reactive intermediate. The study is important because it demonstrates that mere observation of an adsorbed intermediate, or even monitoring its qualitative behavior, at reaction conditions is not sufficient to prove that it has a role in the reaction mechanism. To demonstrate that it is a reaction intermediate it is necessary to show quantitatively that it's dynamic behavior is consistent with the overall reaction rate measured at the same conditions. The need for dynamic in situ experiments to obtain information on reaction mechanisms was first stated by Tamaru [4–6]. The system investigated here is pyridine hydrodenitrogenation (HDN) studied over a nickel phosphide catalyst (Ni_2P/SiO_2) at 423 K and atmospheric pressure. Phosphides have attracted attention because of their high activity in HDN and the related hydrodesulfurization (HDS) reaction [7–14].

The subject of HDN, the removal of nitrogen from petroleum feedstocks, is currently of importance in the production of clean fuels. Combustion of fossil fuels lead to emission of particulate matter, SO_x, NO_x, olefins and aromatics that poison exhaust control devices and contribute to the production of acid rain, smog and atmospheric ozone [15,16]. Recently enacted environmental regulations have made removal of sulfur and nitrogen a focal concern for the refining industry [17]. The subject has been recently reviewed [18,19].

The removal of nitrogen compounds from petroleum crudes by hydrodenitrogenation (HDN) occurs simultaneously with other catalytic hydrotreating processes. Although the nitrogen content in petroleum crudes is generally 5 to 20 times lower than the sulfur content, compared to sulfur heterocycles, nitrogen compounds are more difficult to hydroprocess [20]. If not removed, basic nitrogen compounds greatly inhibit HDS because of their preferential adsorption on catalytic sites [21]. Thus, the ability to carry out efficient HDN is key to deep HDS as the reaction rate of sulfur

* Corresponding author.
E-mail address: oyama@vt.edu (S.T. Oyama).

0021-9517/$ – see front matter
doi:10.1016/j.jcat.2009.02.028

removal is markedly inhibited by small amounts of basic nitrogen compounds in the range 0–50 ppm [22–24]. The inhibition is most pronounced for hydrogenation sites because of strong adsorption on these centers [25–27], and minimizing the inhibiting effect by the efficient removal of nitrogen is vital to achieve low levels of sulfur. As a result, detailed study of HDN mechanisms and surface kinetics of adsorbed nitrogen compounds is important for the development of improved catalysts for HDN.

Previous studies in our group have employed in situ Fourier transform infrared spectroscopy (FTIR) to probe the nature of active sites and adsorbed intermediates on the surfaces of conventional and novel hydrotreating catalysts [13]. The FTIR spectra in He of pyridine adsorbed on $NiMoS/Al_2O_3$ and Ni_2P/SiO_2 showed similar features that were assigned to the presence of a surface pyridinium species on both catalysts. When the flow was switched to H_2, the pyridinium species on Ni_2P/SiO_2 was hydrogenated and the presence of a piperidinium species was observed. However, on $NiMoS/Al_2O_3$ little change occurred in the spectrum. These observations were attributed to the high hydrogenation activity of Ni_2P/SiO_2 as compared to the conventional hydrotreating catalyst $NiMoS/Al_2O_3$ [11–14]. The question arises as to the kinetic role of the adsorbed pyridinium species under reaction conditions. It is desirable to determine whether the pyridinium surface species is a true reaction intermediate or if it exists on the catalyst surface as a spectator, with no role in the overall HDN kinetics. The analysis of coverage under transient conditions (ACT) shows that pyridinium ions react about 100 times slower than the steady-state rate of reaction, indicating that they do not participate in the reaction pathway.

2. Experimental

2.1. Synthesis and characterization

The catalyst used in this study was a nickel phosphide (Ni_2P) supported on silica (Cabosil, EH-5 grade). The phosphide was prepared with excess phosphorous (Ni/P = 1/2) and a loading of 1.15 mmol Ni/g support (12.2 wt% Ni_2P/SiO_2). The catalyst precursors were nickel nitrate hexahydrate, $Ni(NO_3)_2{\cdot}6H_2O$ (Aesar, 99%), and ammonium hydrogen phosphate, $(NH_4)_2HPO_4$ (Aldrich, 99%). The chemicals used in the study of pyridine hydrodenitrogenation were pyridine (Aesar, 99.5+% spectrophotometric grade), piperidine (Aldrich, 99.9%), *n*-nonane (Aesar, 99%) and *n*-tridecane (Aesar, 99%). All chemicals were used as received. The gases employed were He (Airgas, UHP grade), H_2 (Airgas, UHP grade), N_2 (Airgas, UHP grade) and CO (Linde Research Grade, 99.97%). The gases were passed through two-stage gas purifiers (Alltech, Model 4658) to remove moisture and oxygen. Additionally, 0.5% O_2/He (Airgas, UHP grade), which was used for passivation of reduced samples, was passed through a purifier to remove moisture.

The synthesis of the supported catalyst involved two steps and was reported previously [28–30]. Briefly, in the first step, a supported nickel phosphate was prepared by incipient wetness impregnation of nickel and phosphorous precursors, followed by drying at 393 K for 6 h and calcination at 673 K for 4 h. In the second step, the phosphate was reduced to a phosphide by temperature-programmed reduction (TPR). After the temperature program, the sample was cooled to room temperature in flowing He and passivated in a flow of 0.5% O_2/He for 4 h.

The Ni_2P/SiO_2 catalyst and blank SiO_2 were characterized by BET surface area measurements (Micromeritics ASAP 2010), CO chemisorption and powder X-ray diffractometry (XRD, Scintag XDS-2000 operated at 45 kV and 40 mA with Cu-K_α monochromatized radiation). Irreversible CO uptake measurements were obtained using a flow technique on re-reduced passivated samples and were used to titrate the surface metal atoms and provide an estimate of active sites on the catalyst. The CO uptake amounts were used to calculate turnover frequencies in the steady-state kinetic measurements.

2.2. Spectroscopic and kinetic measurements

Transmission infrared spectra of pyridine adsorbed on Ni_2P/SiO_2 and blank SiO_2 were collected with a combined in situ reactor–spectrometer system (Fig. 1). Fourier transform infrared (FTIR) spectra were collected with a spectrometer (Digilab Excalibur Series FTS 3000) equipped with a liquid N_2-cooled mercury–cadmium–telluride detector. The low volume (~20 cm^3) in situ reactor was equipped with water cooled KBr windows, connections for inlet and outlet flows, and thermocouples connected to a temperature controller to monitor and control the sample temperature. For all experiments, 25 mg of finely ground Ni_2P/SiO_2 or blank SiO_2 were pressed into self-supporting wafers with a diameter of 13 mm (18.8 mg/cm^2) and were mounted vertically in a quartz sample holder. Rods of CaF_2 (13 mm diameter) were placed on both sides of the sample to minimize interference of gas phase pyridine and to reduce the dead volume of the reactor.

Studies of pyridine adsorption and reaction on Ni_2P/SiO_2 and blank SiO_2 at several temperatures were used to confirm the identity and determine the stability of the adsorbed pyridinium intermediate. For these experiments, absorbance spectra were collected in the range 4000–1000 cm^{-1} at a resolution of 4 cm^{-1} with 64 scans/spectrum. Before dosing pyridine, the Ni_2P/SiO_2 and blank SiO_2 samples were pretreated in H_2 for 2 h at 723 K at a flow rate of 82 μmol/s (120 cm^3/min). After reduction, the samples were slowly cooled in flowing He or H_2 (140 μmol/s, 200 cm^3/min) and background spectra were collected in the absence of pyridine at 523, 473, 423, and 373 K. The samples were dosed at atmospheric pressure and 373 K with 1.0 mol% pyridine in He or H_2 carrier at the same flow rate (140 μmol/s, 200 cm^3/min) until saturation was achieved. The carrier gas was passed through a pyridine-filled bubbler immersed in a temperature-controlled water bath held at 298 K. The Antoine equation was used to obtain the pyridine vapor pressure (2.81 kPa at 298 K):

$$\log P^{\mathrm{sat}} = A - \frac{B}{T + C}, \tag{1}$$

where P^{sat} is the vapor pressure in mm Hg, T is the bubbler temperature in °C and the coefficients are 7.1874, 1463.63 and 224.598 for A, B and C, respectively [31]. The concentration of pyridine was adjusted by blending the main carrier flow containing pyridine with a dilution gas while keeping the total flow rate constant at 200 cm^3/min.

The samples were then purged with carrier gas for 300 s to remove gaseous and weakly adsorbed pyridine. Spectra are shown with subtraction of the background contribution to highlight the pyridine adsorbate peaks. Spectra were acquired at 373, 423, 473, 573 and 673 K with a heating rate of 0.083 K/s (5 K/min). The reactor temperature was held constant at each temperature for 180 s to collect the corresponding spectrum.

Transient kinetic experiments were performed to ascertain the kinetic role of the pyridinium surface species by measuring the rate of reaction of the adsorbed pyridine intermediate. FTIR spectroscopy was used to directly monitor the evolution of pyridinium coverage with respect to time at atmospheric pressure and 423 K. For these experiments, absorbance spectra were collected in multi-scan mode in the range 4000–1000 cm^{-1} at a resolution of 4 cm^{-1}. Spectra were collected every 6 s with 10 scans/spectrum. Before all measurements, the self-supporting Ni_2P/SiO_2 wafers were pretreated as before. After the reduction, the samples were cooled in flowing He or H_2 (200 cm^3/min) to 423 K and background spectra were collected. The flow was then quickly switched

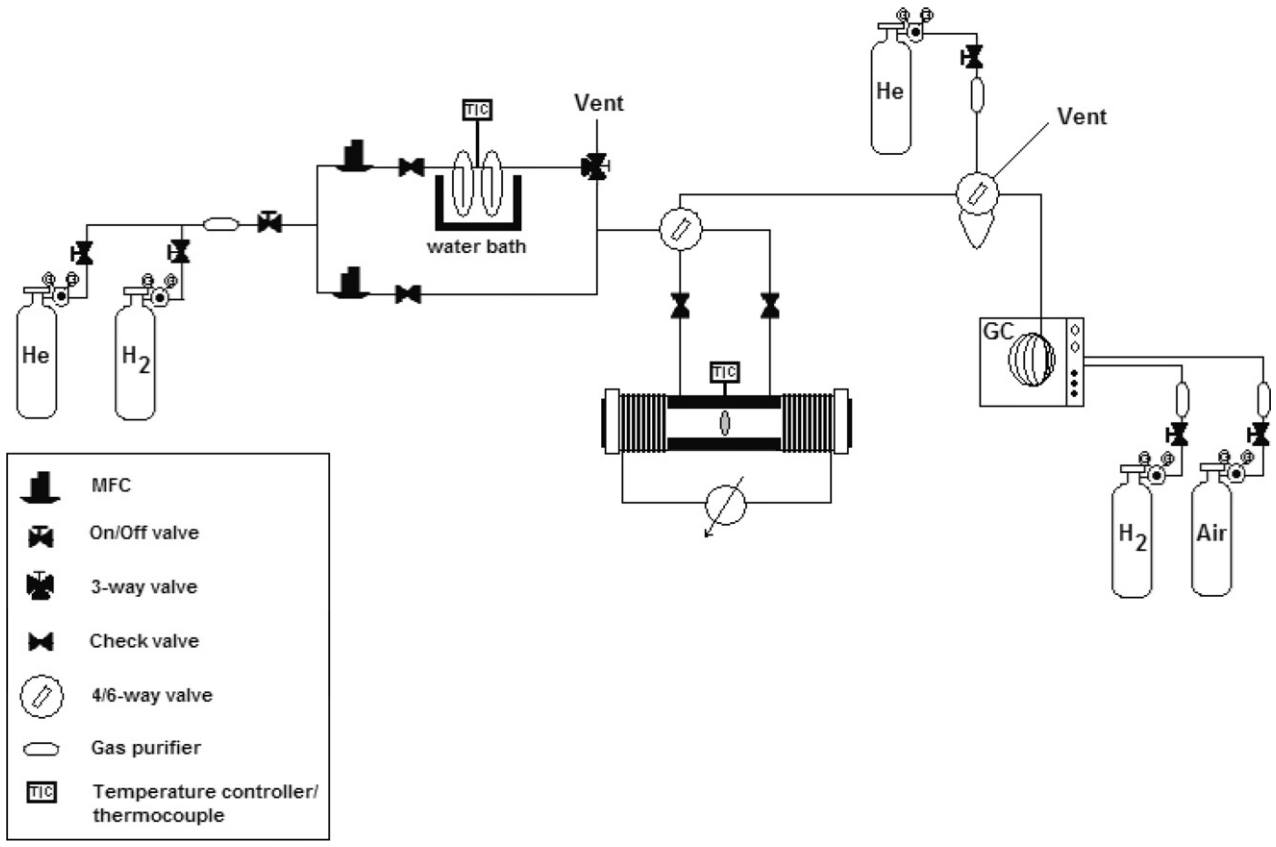

Fig. 1. In situ FTIR reactor system.

Table 1
Pyridine weight times for gas-phase transient kinetic experiments.

Carrier gas flow rate (cm^3 (NTP) min^{-1})	Pyridine flow rate $\times 10^3$ (mol h^{-1})	Pyridine concentration (mol%)	Weight time (g h mol^{-1})
15	1.1	0.21	24
30	2.1	0.43	12
45	3.2	0.64	7.9
60	4.2	0.85	6.0
75	5.2	1.1	4.8
90	6.3	1.3	4.0

to pyridine and carrier gas at a total flow rate of 200 cm^3/min and collection of spectra was initiated. All measurements were started with a clean sample surface and continued until steady-state coverage of pyridine was attained. Vapor-phase concentrations of pyridine were varied to measure the reaction rates over a range of weight times. The weight time (g h/mol) is a measure of contact time and was calculated with the following equation:

$$\text{Pyridine weight time} = \frac{W_{\text{catalyst}}}{\dot{F}_{\text{pyridine}}}, \tag{2}$$

where W_{catalyst} is the mass of catalyst (0.025 g) and $\dot{F}_{\text{pyridine}}$ is the molar flow rate of pyridine in mol/h. Table 1 summarizes the flow rates and weight times that were used in the transient kinetic experiments.

For each spectrum a peak at 1491 cm^{-1}, corresponding to pyridine ring vibrations on Brønsted and Lewis acid sites (mode ν_{19b}) of Ni_2P/SiO_2, was monitored as a function of time. The areas of the peak were converted to fractional coverage by separate calibration experiments to determine the area corresponding to full coverage ($\theta = 1$). Measurements at a lower temperature (273 K) indicated that room temperature was adequate for achieving saturation coverage of pyridine. Briefly, for the calibrations the Ni_2P/SiO_2 catalyst sample was pretreated as mentioned above and a background spectrum was collected at 298 K. The sample was then dosed with successively higher concentrations of pyridine in He flow until the peak area (1491 cm^{-1}) was constant.

For both the calibration and transient kinetic experiments, slight differences in wafer thicknesses were reconciled by normalizing by the areas of the ν_{OH} stretching frequencies of the SiO_2 support. The ν_{OH} frequencies, which were recorded in the background spectra before exposure to pyridine, were found in the 4000–3200 cm^{-1} region of the spectra.

The overall turnover rates of pyridine were measured in a three-phase trickle-bed reactor (Fig. 2). The reactor has a concentric tubular design with an outer stainless steel body and an inner quartz sleeve which prevented contact of the catalyst with the stainless steel. The tight-fitting quartz sleeve (18 mm o.d., 15 mm i.d.) was sealed at the top of the reactor with compression fittings but was loose at the bottom to allow pressure equalization. The length of the experiments required the use of exchangeable H_2 cylinders. The flow of the gas and liquid reactant mixture entered from the top and passes through Pyrex beads for preheating and good flow dispersion. The catalyst was held by quartz wool plugs, and an axial thermocouple in a quartz sheath was used to measure the temperature of the catalyst bed. The reactor was heated with a furnace and the temperature of the catalyst bed was controlled with a temperature controller. The liquid feed was metered from burettes with a high-pressure liquid pump (Lab Alliance, Model Series I) and H_2 flow was delivered by mass flow controllers (Brooks, Model 5850E). The reactant passed over the catalyst bed in downflow mode and into a water-cooled separation/sampling system. Samples were collected every 2 or 3 h in sealed septum vials and were analyzed off-line with a gas chromatograph (Hewlett-Packard, 5890A) equipped with a 0.32 mm i.d. × 50 m fused silica capillary column (CPSil-5CB, Chrompack, Inc.) and a flame ionization detec-

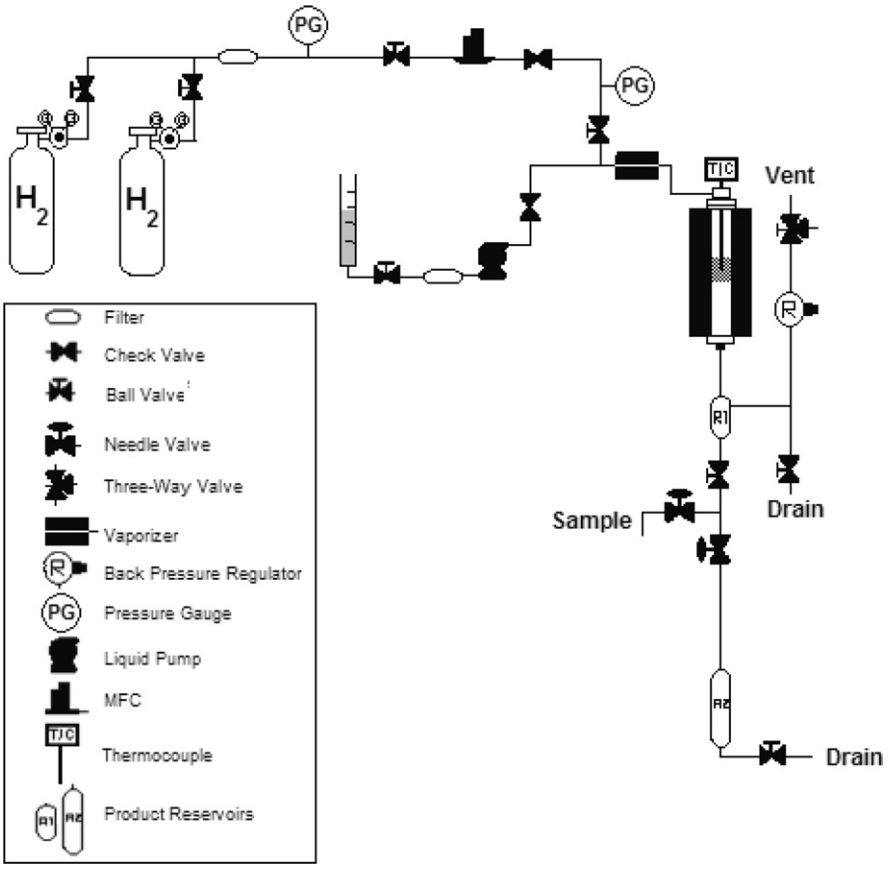

Fig. 2. Three-phase trickle bed reactor system.

tor. Reactants and products were identified by matching retention times to standards injected separately.

For the measurements of the turnover rates of pyridine, the system was operated at 423 K and atmospheric pressure with a liquid feed containing 20000 ppm wt (2.0 wt%) N as pyridine, 20000 ppm wt (2.0 wt%) *n*-nonane as internal standard and balance *n*-tridecane as solvent. The Ni_2P/SiO_2 catalyst was in pelletized form (16/20 mesh) and was supported between quartz wool plugs. A quantity of 0.100 g of sample was charged to the reactor and diluted with SiC to a total bed volume of 8 cm^3 to ensure plug flow conditions. The remaining volume of the reactor was filled with 3 mm Pyrex beads. Prior to the kinetic measurements, the sample was pretreated at 723 K for 2 h under 120 cm^3/min of flowing H_2 at atmospheric pressure. After reduction, the reactor was cooled to 423 K and the H_2 flow rate was increased to 140 μmol/s (200 cm^3/min). Liquid feed was then introduced and the reaction was allowed to stabilize for 25 h before sampling. Additionally, the system was allowed to run for 25 h after every change in flow rate. Flow rates of the feed were varied to match the weight times used in the transient FTIR experiments. The overall turnover frequency was obtained from the following formula:

$$\mathrm{TOF} = \frac{\text{pyridine flow rate (μmol/s)} \cdot \text{steady-state conversion}}{\text{catalyst weight (g)} \cdot \text{chemisorption uptake (μmol/g)}}, \qquad (3)$$

where the catalyst weight was 0.100 g for all experiments. The results from several samples were averaged to determine the steady-state conversion at each weight time. Table 2 summarizes the pyridine flow rates employed in the kinetic measurements.

Table 2
Pyridine weight times for steady-state kinetic experiments.

Pyridine flow rate $\times 10^3$ (mol h^{-1})	Weight time (g h mol^{-1})
7.3	14
9.3	11
15	6.6
20	5.0

Table 3
Physical properties of Ni_2P/SiO_2 catalyst.

	BET surface area (m^2 g^{-1})	CO uptake (μmol g^{-1})	Metal dispersion (%)	Particle size (nm)
Ni_2P/SiO_2	148 (333)[a]	90	8	11

[a] BET surface area of the blank SiO_2 support.

3. Results

The BET specific surface area and CO chemisorption uptake of the supported Ni_2P sample are listed in Table 3. As stated earlier, the CO uptake value was used to calculate turnover frequencies in the steady-state kinetic experiments. The BET surface area was much lower than that of the blank support. This is likely due to sintering at the elevated temperatures used in the synthesis.

Fig. 3 shows the powder XRD pattern of the reduced Ni_2P/SiO_2 catalyst after reduction and passivation. The pattern exhibits a broad peak at $2\theta \sim 22°$ due to the amorphous SiO_2 support. At higher angles the XRD pattern for Ni_2P/SiO_2 confirms the formation of the Ni_2P phase with peaks at $2\theta \sim 41°$, 45°, 48° and 55° due to the Ni_2P phase (bottom panel). The phase corresponds to hexagonal Ni_2P which adopts the Fe_2P structure with space group $P_{\bar{6}2m}$ [32]. The pattern of a reference Ni_2P from the powder diffraction file (PDF 3-953) is also presented [33].

Fig. 4 shows the FTIR spectrum of 0.85 mol% pyridine in He carrier adsorbed on Ni_2P/SiO_2 at 423 K. The left panel shows the high wavenumber region of the spectrum and the right panel highlights

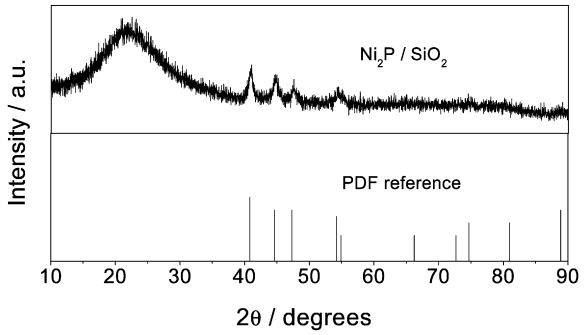

Fig. 3. Powder XRD pattern of Ni_2P/SiO_2 catalyst sample.

the low wavenumber region. Included in the figures are peak positions and band assignments, where BPY, LPY, HPY and PPY signify pyridine interacting with Brønsted acid sites (BPy), Lewis acid sites (LPy), hydrogen-bonded pyridine (HPy), and physisorbed pyridine (PPy), respectively. Table 4 summarizes the observed vibrational frequencies and assignments, which are presented in detail in the discussion section. In the high wavenumber region, the main spectral features include two negative peaks at 3745 and 3669 cm^{-1} and three positive features centered at 3143, 3079 and 3046 cm^{-1}. In this figure, as well as in others in this study, background spectra were subtracted as explained in the experimental section, and this gives rise to the negative peaks. In the low wavenumber region the main spectral features are located at 1638, 1607, 1595, 1576, 1547, 1491, 1447 cm^{-1}, with the latter displaying a shoulder at ~1433 cm^{-1}.

Fig. 5 shows the FTIR spectrum of 0.85 mol% pyridine in H_2 carrier adsorbed on Ni_2P/SiO_2 at 423 K. The spectra appear similar to those obtained for pyridine adsorbed on Ni_2P/SiO_2 in He flow. In the high wavenumber region, the two negative peaks at 3745 and 3669 cm^{-1} are again present, and in the low wavenumber region, the peaks located at 1638 and 1547 cm^{-1} are again observed and appear unchanged. However, there are several important differences. The peaks in the 3200–2800 cm^{-1} region are shifted to slightly lower wavenumbers and two new weak features centered at 2957 and 2874 cm^{-1} are now visible. In the low wavenumber region the intensities of the features located at 1491 and 1447 cm^{-1} are slightly attenuated. The intensity of the peak at 1607 cm^{-1} is much lower than the corresponding peak observed under He flow and appears as a shoulder on the peak at 1595 cm^{-1}. Under H_2 flow, a new unidentified peak with strong

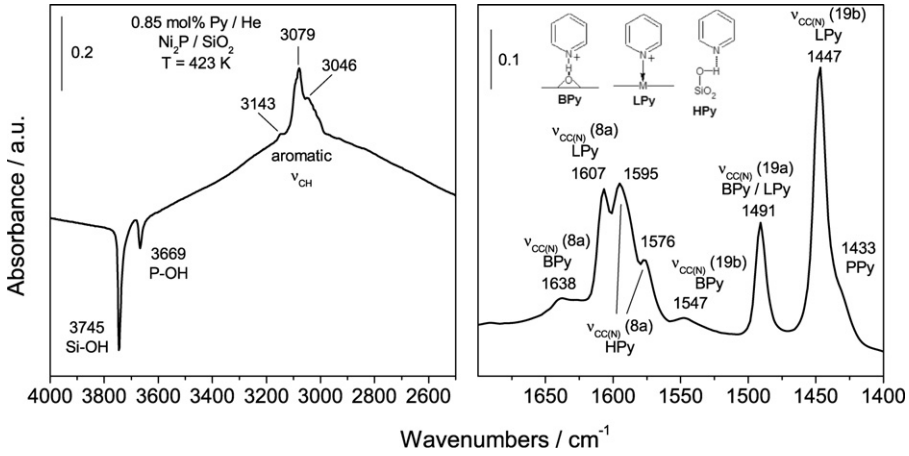

Fig. 4. FTIR spectrum of 0.85 mol% pyridine in He flow adsorbed on Ni_2P/SiO_2 at 423 K. BPY, LPY, HPY and PPY signify pyridine interacting with Brønsted acid sites (BPy), Lewis acid sites (LPy), hydrogen-bonded pyridine (HPy) and physisorbed pyridine (PPy), respectively.

Table 4
Summary of FTIR band assignments (cm^{-1}).

Pyridine				Tetrahydro-pyridine	Piperidine	Assignment
Brønsted	Lewis	H-bonded	Physisorbed			
BPy	LPy	HPy	PPy	THP	PIP	
						3745 Si–OH, ν_{OH}
						3669 P–OH, ν_{OH}
		3143–3188				Aromatic C-H, ν_{CH}
		3079–3075				Aromatic C–H, ν_{CH}
		3046–3038				Aromatic C–H, ν_{CH}
				2957	2943, 2864	Aliphatic C–H, ν_{CH}
				2874	2806, 2739	Aliphatic C–H, ν_{CH}
					1620	Scissoring NH_2, ν_{NH_2}
1638	1607	1595,1576	~1607[a]			Ring breathing, ν_{CCN} (8a)
1547	1491	~1547[a]	1433	1481	1474	Ring breathing, ν_{CCN} (19b)
1491	1447	~1491[a]	~1447[a]			Ring breathing, ν_{CCN} (19a)
					1458	ν_{CN}
					1450	ν_{HPip}

[a] No distinct band seen, possible overlap with the indicated band.

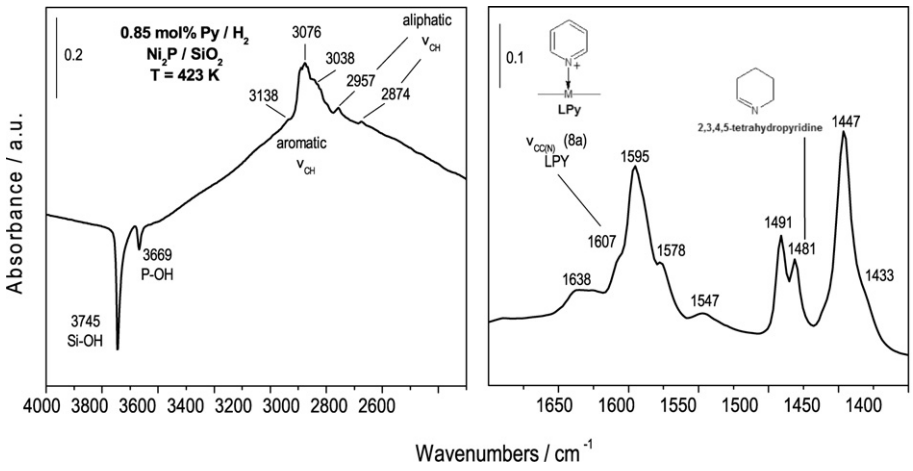

Fig. 5. FTIR spectrum of 0.85 mol% pyridine in H_2 flow adsorbed on Ni_2P/SiO_2 at 423 K.

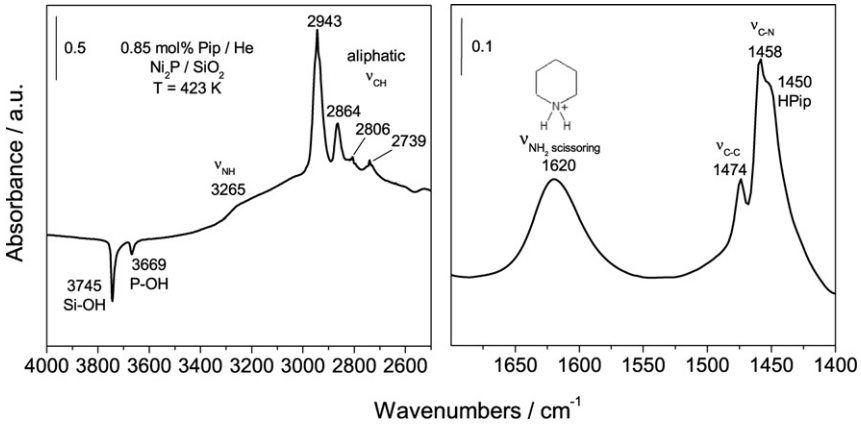

Fig. 6. FTIR spectrum of 0.85 mol% piperidine in He flow adsorbed on Ni_2P/SiO_2 at 423 K.

intensity is observed at 1481 cm^{-1}. The new feature overlaps with the peak at 1491 cm^{-1} but is clearly observed, even at low concentrations of pyridine in H_2 carrier, but never under He. The feature is assigned to a partially hydrogenated pyridine molecule. Assignments are summarized in Table 4.

In order to probe the identity of the peak at 1481 cm^{-1}, piperidine at a concentration of 0.85 mol% in He carrier was adsorbed on the Ni_2P/SiO_2 catalyst at 423 K, as shown in Fig. 6. The spectrum for piperidine on Ni_2P/SiO_2 is substantially different from that for pyridine. In the high wavenumber region, two negative peaks are again observed at 3745 and 3669 cm^{-1}. A prominent shoulder on a rising background was also located at ~3265 cm^{-1}. No bands in the 3200–3000 cm^{-1} region of the spectrum are observed but several strong peaks below 3000 cm^{-1} are centered at 2943, 2864, 2806 and 2739 cm^{-1}. In the low wavenumber region there is a new broad feature centered at 1620 cm^{-1} and two strong, overlapping peaks located at 1474 and 1458 cm^{-1}, with the latter displaying a prominent shoulder at ~1450 cm^{-1}. Assignments are summarized in Table 4. As will be discussed, all these features are due to a piperidinium ion. Upon switching the carrier flow to H_2, no significant changes in the spectrum were observed.

Fig. 7 shows the FTIR spectra of pyridine adsorbed on the blank SiO_2 support under He flow as a function of temperature. The main spectral features are located at 3748, 3738, 3090, 3078, 3044, 3021, 1593, 1575, 1445 and 1433 cm^{-1}. The absorbance peaks at 3748 and 3738 cm^{-1} appear as negative features. For all spectra, because of the background subtraction a decrease in the intensity of a negative peak with increasing temperature indicates growth of the peak and an increase in the concentrations of the corresponding surface functionalities. The opposite applies to positive features in the spectra. As the temperature is increased to 523 K the intensities of all positive features in the spectra decrease, and so do the corresponding concentrations.

Fig. 8 shows the FTIR spectra of pyridine adsorbed on Ni_2P/SiO_2 under He flow after degassing. The main spectral features are centered at 3745, 3669, 3143, 3079, 1638, 1607, 1595, 1576, 1547, 1491 and 1447 cm^{-1}. The spectra appear similar to pyridine adsorbed on blank SiO_2, but several new peaks are now present. The two negative features at 3748 and 3738 cm^{-1} observed in Fig. 7 now appear as a single band that is shifted to slightly lower wavenumbers at 3745 cm^{-1}. A second, weaker negative peak at 3669 cm^{-1} is again prevalent at slightly lower wavenumbers. The peaks in the 3200–3000 cm^{-1} region are again present on a rising background and are shifted to slightly higher wavenumbers. In the low wavenumber region several new peaks are present at 1638, 1607 and 1547 cm^{-1} and a strong new feature at 1491 cm^{-1}. The peaks previously observed for pyridine adsorption on SiO_2 are shifted to higher wavenumbers at 1595, 1576 and 1447 cm^{-1}. The intensities of all features decrease as the temperature is increased up to 523 K.

Fig. 9 shows the FTIR spectra of pyridine adsorbed on Ni_2P/SiO_2 under H_2 flow after degassing. The main spectral features are located at 3745, 3669, 3143, 3079, 2984, 2951, 2872, 1638, 1607, 1597, 1578, 1559, 1542, 1491 and 1447 cm^{-1}. The spectra are very similar to those obtained under He flow. In the high wavenumber region the intensity of the negative peak at 3669 cm^{-1} is slightly attenuated and several new peaks appear at 2984, 2951 and 2872 cm^{-1}. At higher temperatures, a shoulder on the peak

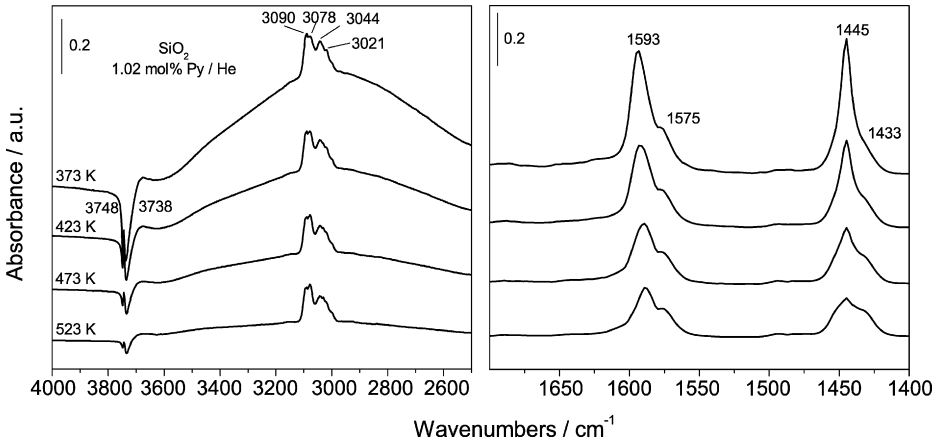

Fig. 7. FTIR spectra of pyridine adsorbed on SiO_2 in He flow as a function of temperature.

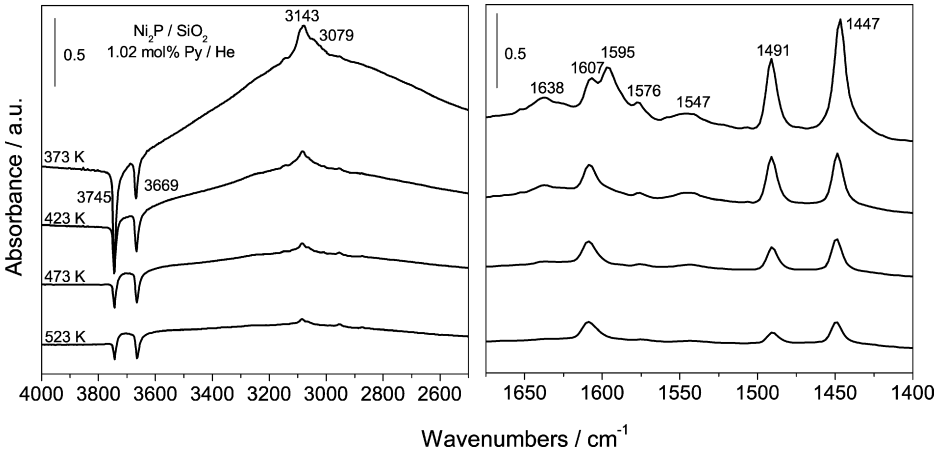

Fig. 8. FTIR spectra of pyridine adsorbed on Ni_2P/SiO_2 in He flow as a function of temperature.

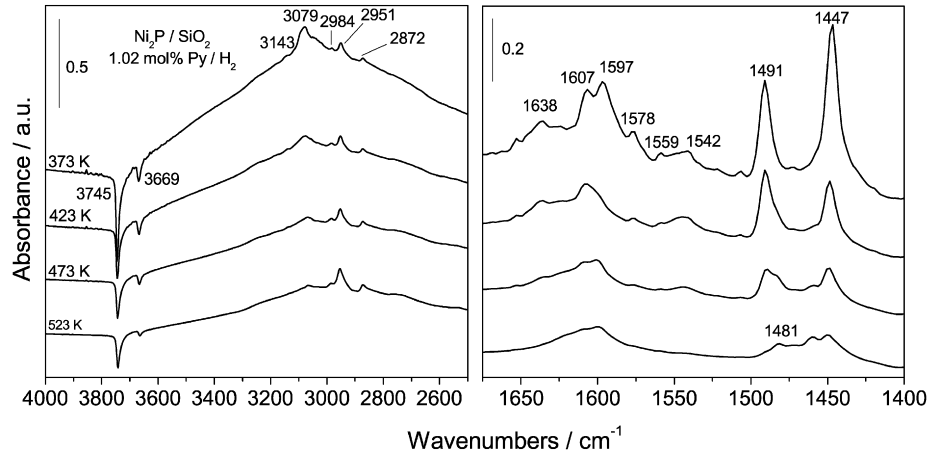

Fig. 9. FTIR spectra of pyridine adsorbed on Ni_2P/SiO_2 in H_2 flow as a function of temperature.

at 1491 cm^{-1} becomes visible at approximately 1481 cm^{-1}. With increasing temperature, the intensity of this peak increases up to 523 K concomitantly with the peaks at 2984, 2951 and 2872 cm^{-1}. Additionally, a peak at 1460 cm^{-1} becomes visible at 473 K and grows in intensity with further heating to 523 K. The intensities of all other features are observed to decrease with heating.

Fig. 10a represents the time-resolved spectra for the adsorption of 0.85 mol% pyridine in He carrier on Ni_2P/SiO_2 at 423 K. As soon as pyridine was introduced, the intensity and area of the peak at 1491 cm^{-1} increased rapidly and reached a steady value after ~200 s. Fig. 10b represents the time-resolved spectra for the adsorption and reaction of 0.85 mol% pyridine in H_2 carrier. Again, the peak at 1491 cm^{-1} grew rapidly although with lower intensity and area. Under continuous pyridine/H_2 flow, a second well-resolved peak at 1481 cm^{-1} also developed with increasing time but with relatively lower intensity and area. At higher temperatures, this peak appeared as a shoulder (Fig. 9) in the adsorption experiments performed in a H_2 atmosphere. The intensity of the feature at 1491 cm^{-1} again reached a steady value after ~200 s while the intensity of the peak at 1481 cm^{-1} reached a steady

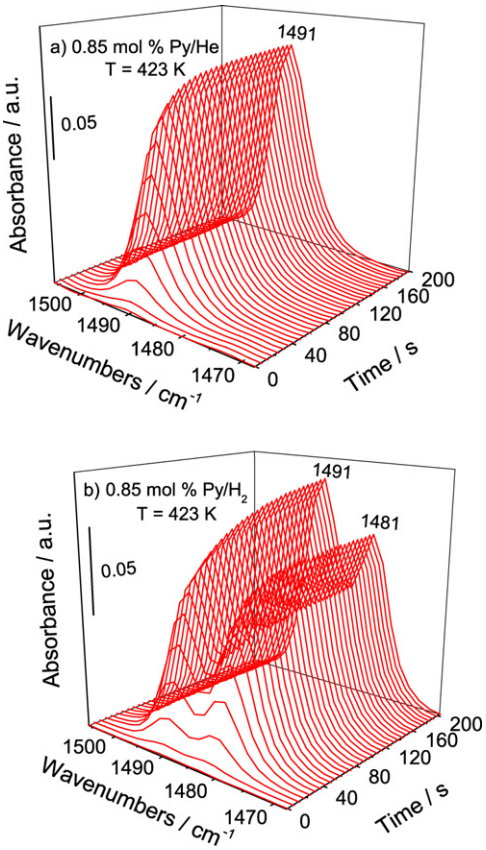

Fig. 10. Time-resolved FTIR spectra of 0.85 mol% pyridine adsorbed on Ni_2P/SiO_2. (a) He carrier at 423 K, (b) H_2 carrier at 423 K.

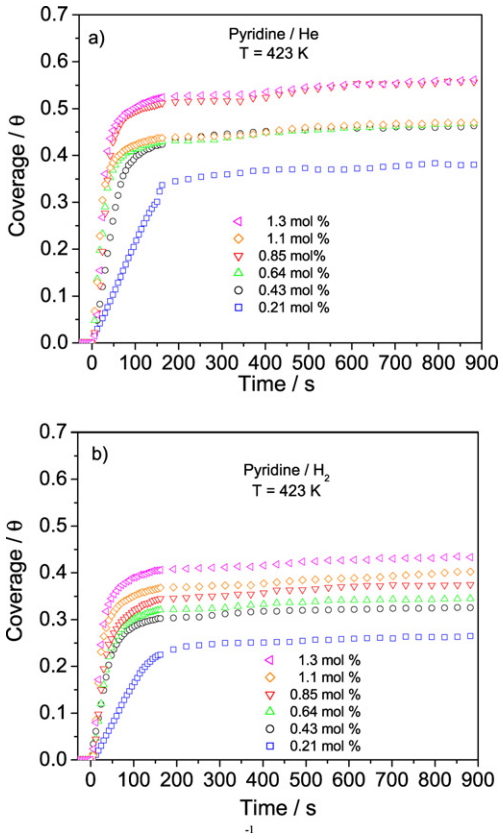

Fig. 11. Transient additions of pyridine (1491 cm^{-1}) at several concentrations over Ni_2P/SiO_2. (a) He carrier at 423 K, (b) H_2 carrier at 423 K.

value in a shorter time of <100 s. As will be discussed, the species giving rise to the feature at 1491 cm^{-1} is not a reactive intermediate in the system. The species associated with the peak at 1481 cm^{-1} may be an actual intermediate in the reaction.

The peak centered at 1491 cm^{-1} was fit with peak-fitting software (Origin 6.1) using a Gaussian curve. Furthermore, the overlapping peaks acquired under H_2 flow were deconvoluted using a multipeak fitting algorithm available with the software. In all cases, the positions of the peaks and their full widths at half maximum were kept constant while other fitting parameters were allowed to vary in the fitting algorithm. The areas of the peak located at 1491 cm^{-1} were converted to fractional coverage from the calibration of the signal at saturation at room temperature. Fig. 11a shows coverage versus time curves for adsorption of pyridine at several concentrations in He on the Ni_2P/SiO_2 catalyst at 423 K. At all concentrations, the coverages of adsorbed pyridine rapidly increased with the introduction of pyridine at time zero and reached steady-state values in ~200 s. Steady-state coverages were obtained for pyridine concentrations of 0.21, 0.43, 0.64, 0.85, 1.1, and 1.3 mol%, respectively. The coverages increased from 0.38 to 0.56, with some variation due to experimental error. Fig. 11b shows the adsorption of pyridine at several concentrations in H_2 carrier on the Ni_2P/SiO_2 catalyst at 423 K. As in He, the coverages of adsorbed pyridine increased rapidly and reached steady-state values in ~200 s. The steady-state coverages increased from 0.26 to 0.43 as the pyridine concentrations increased from 0.21 to 1.3 mol%, respectively. The steady-state coverages of pyridine in H_2 flow were lower than those observed under He flow, as might be expected from reaction.

Table 5 presents the results of the reaction of pyridine over Ni_2P/SiO_2 under steady-state conditions. As expected, the pyridine conversion decreased with decreasing weight time (increasing flow rate). Additionally, the major product observed at all weight times was piperidine. At the highest weight time, a small amount of HDN products were observed. This indicates that further reaction of piperidine was relatively slow at 423 K and atmospheric pressure. Equation (3) was used to calculate pyridine turnover frequencies at each weight time

Table 5
Steady-state pyridine reaction results at 423 K.

Pyridine flow rate (μmol s^{-1})	Pyridine weight time (g h mol^{-1})	Conversion (%)	Turnover frequency, TOF (s^{-1})	Piperidine selectivity (%)
2.0	14	45	0.102	99
2.6	11	37	0.106	100
4.2	6.6	25	0.117	100
5.5	5.0	21	0.130	100

4. Discussion

4.1. Previous studies of pyridine HDN

The main subject of this paper is the study of reaction mechanisms by a method called analysis of coverage transients (ACT) method, which will be presented shortly. The method is applied to the hydrodenitrogenation (HDN) of pyridine and it is appropriate to first provide background in the area of HDN. Pyridine, a six-membered nitrogen heterocycle, is a classic probe molecule and is the simplest basic nitrogen compound for studying HDN. A considerable number of studies have been conducted on the mechanism of pyridine HDN. In general, the denitrogenation of heterocyclic nitrogen compounds is preceded by hydrogenation of the aromatic heterocyclic ring in order to convert strong aromatic C–N bonds into weaker aliphatic C–N bonds. Subsequent removal of nitrogen

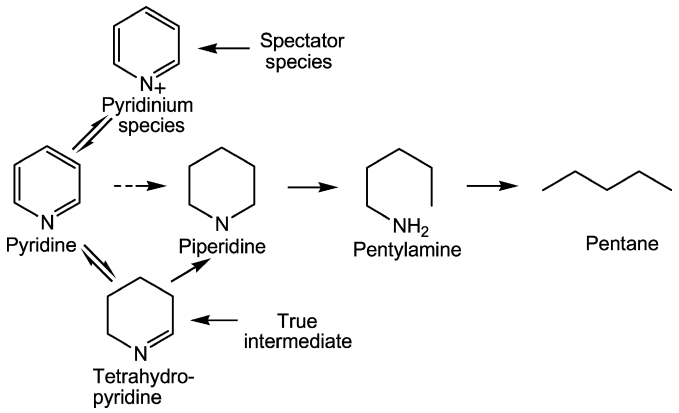

Scheme 1. Simplified reaction pathway for pyridine HDN.

proceeds by cleavage of a C–N bond to form an amine intermediate followed by removal of nitrogen to yield hydrocarbons and NH_3. It has been documented that the pyridine HDN reaction follows an established sequence of steps as shown in Scheme 1, which will be discussed in further detail later. The main steps include hydrogenation of the heterocyclic aromatic ring to yield piperidine, ring opening by cleavage of one C–N bond and subsequent removal of nitrogen from *n*-pentylamine as NH_3 [34,35]. However, Ledoux et al. showed that ring opening is possible prior to complete saturation of the heterocyclic aromatic ring [36]. More complex reaction networks have been proposed which included disproportionation reactions of saturated products to form *N*-pentylpiperidine, though condensation products were only observed at high temperatures and pressures [37,38].

Polycyclic aromatic nitrogen compounds such as quinoline and carbazole are among the most refractory nitrogen compounds. Quinoline has a double ring structure containing a benzene ring fused to pyridine at adjacent carbon atoms. Similarly, carbazole possesses a triple ring structure with two carbocyclic rings bonded to the adjacent carbon atoms of pyrrole. The reactions involved in the HDN of polycyclic nitrogen compounds involve hydrogenation of the nitrogen heteroring, hydrogenation of the benzenic ring(s) and C–N bond cleavage [35]. Details of the mechanisms of quinoline HDN has been studied extensively by Prins and coworkers [39,40] and carbazole HDN by Abu and Smith [41,42]. The HDN of these molecules proceeds through multiple parallel pathways involving hydrogenation and hydrogenolysis of C–N bonds. However, the HDN of all nitrogen heterocycles entails the common steps of heterocyclic ring hydrogenation, ring opening and the final removal of nitrogen as NH_3. As a result, study of the HDN of pyridine or pyrrole can be used to investigate the essential steps of HDN.

Recently, new insight was provided on the HDN mechanism by Prins and coworkers [43] in a study on 2-methylpyridine and 2-methylpiperidine HDN over sulfided NiMo/γ-Al_2O_3. The HDN of 2,3,4,5-tetrahydro-6-methylpyridine, which was previously reported as an intermediate in the hydrogenation/dehydrogenation of 2-methylpyridine/2-methylpiperidine, was examined [44]. The study concluded that 2-methylpyridine is hydrogenated to 2-methylpiperidine and that both amines react to form partially hydrogenated intermediates, the imines 2,3,4,5-tetrahydro-2-methylpyridine and 2,3,4,5-tetrahydro-6-methylpyridine with a single C=N bond. Ring opening of the imines occurs by addition of H_2S, elimination, and hydrogenation to form amino-hexanethiols. Subsequently, the thiols react by hydrogenolysis to hexylamines, and the second C–N bond is cleaved by hexylimine formation, H_2S addition and elimination of NH_3. As a result, the imines were proposed to be intermediates of both hydrogenation and denitrogenation. The proposed reaction sequence is different from those given in previous studies in which a direct reaction of 2-methylpiperidine to ring-opened products was assumed (Scheme 1, dashed arrow).

The reaction rates of the first steps (Scheme 1), hydrogenation of the aromatic ring and ring-opening, are of similar order of magnitude and slow relative to subsequent steps in the mechanism. Several studies have observed a pyridine–piperidine thermodynamic equilibrium under conventional HDN conditions, suggesting that aromatic ring hydrogenation is fast compared to ring-opening [45–47]. Still yet, many studies have provided evidence for either step being rate-limiting and for the slow step to depend on the amine and experimental conditions such as catalyst properties, temperature, pressure and H_2S/H_2 ratio [12,48–52].

Pyridine adsorption is often studied with in situ Fourier transform infrared spectroscopy (FTIR) to probe the surface acidic properties of supports and catalysts. Characteristic bands in the FTIR spectrum are used to determine if pyridine is protonated through the nitrogen atom by surface Brønsted acid sites and/or bonded to coordinative unsaturated metal sites (Lewis acid sites). Upon interaction with a Brønsted acid site, pyridine is protonated to a pyridinium ion with specific IR features around 1545–1540 cm^{-1}. Interaction of pyridine with a Lewis acid site leads to a coordinatively bonded pyridinium complex with a well-resolved band centered around 1452–1447 cm^{-1}. A band located around 1490 cm^{-1} is common to both adsorbed species. In addition, the different pyridine–acid site interactions give rise to other specific absorbances as discussed later. Many studies have employed this technique to qualitatively and quantitatively study the acidic properties of catalytic materials and the resulting effect on catalyst properties and activity [53].

Damyanova et al. investigated changes in the surface acidity upon impregnation of Mo on mixed ZrO_2–SiO_2 and ZrO_2–Al_2O_3 [54]. Rana et al. examined changes in support acidity upon incorporation of MgO, SiO_2, TiO_2 and ZrO_2 with Al_2O_3 [55]. Sánchez-Minero et al. studied pyridine adsorption on Al_2O_3 and Al_2O_3 modified with 10 wt% SiO_2. On pure Al_2O_3 they found the presence of two Lewis acid sites with different strength – Al^{3+} in octahedral and tetrahedral coordination environments. Incorporation of SiO_2 led to partial covering of some Lewis acid sites with only octahedral Al^{3+} sites remaining on the surface [56]. DeCanio and Weissman used pyridine adsorption to correlate HDN activity with surface acidity of boron-modified NiMo/Al_2O_3 catalysts. They determined that nitrogen removal activity was dependent on Brønsted acidity as measured by the pyridinium band at 1540 cm^{-1} [57]. Korányi and coworkers investigated the effects of sulfidation on the acidity of conventional hydrotreating catalysts supported on Al_2O_3 and amorphous SiO_2–Al_2O_3. Sulfidation of the catalyst samples was found to decrease the Brønsted and Lewis acidities of all samples [58]. Navarro and coworkers studied the effects of Ru incorporation on the surface acid properties of conventional hydrotreating catalysts. Introduction of Ru was found to enhance both the Brønsted and Lewis acidities of the samples [59]. Rhee and coworkers employed FTIR measurements of adsorbed pyridine to examine the promoting effects of Ni on Mo/Al_2O_3 and W as a secondary promoter on the acidic properties and HDN activity. Enhancement of HDN activity with addition of Ni was attributed to an improvement of the reducibility of the oxidic Mo/Al_2O_3 sample rather than an increase in Brønsted acidity. Further enhancement of activity with W as a secondary promoter was ascribed to the formation of new Brønsted acid sites [60].

4.2. Spectral interpretation

The ACT method can be used with any spectroscopic technique which can detect adsorbed reaction intermediates. The present study analyzes results from Fourier transform infrared (FTIR) spectroscopy and, before introducing the ACT method, the obtained

data will be discussed. FTIR has been used to characterize Ni_2P catalysts in the past [13,61,62]. The FTIR data for pyridine adsorbed on Ni_2P/SiO_2 are shown in Figs. 4 and 5 and show several common features in both He and H_2 carrier gases. Table 4 summarizes the results and assignments. The negative bands located at 3745 and 3669 cm^{-1} are assigned to hydroxyl vibrations of the SiO_2 support and P–OH of the active phase, respectively [12,13,63]. As a result of the background subtraction, these features appear as negative bands upon interaction of pyridine with the surface hydroxyl groups. The Si–OH band is due to hydrogen-bonded pyridine, primarily on the SiO_2 support. The negative band at 3669 cm^{-1} arises from the Brønsted acidity of surface P–OH functionalities and is attributable to protonation of the pyridine nitrogen atom. In a previous study [13] with a silica surface loaded with phosphate the P–OH band appeared at 3660 cm^{-1}, and for a Ni_2P/SiO_2 surface at 3668 cm^{-1}, so the 3669 cm^{-1} band is tentatively assigned to P–OH groups on the Ni_2P. In addition, the three features located between 3150 and 3030 cm^{-1} correspond to aromatic ν_{CH} modes of pyridine [64].

In the low wavenumber regions of Figs. 4 and 5, the peaks at 1547, 1491 and 1447 cm^{-1} correspond to pyridinium ring breathing modes 19b ($\nu_{CC(N)}$) on Brønsted acid sites (BPy), 19a ($\nu_{CC(N)}$) on Brønsted and Lewis acid sites (LPy), and 19b ($\nu_{CC(N)}$) for pyridine coordinated to Lewis acid sites, respectively [64]. The feature at 1447 cm^{-1} also contains a contribution from pyridine hydrogen-bonded (mode 19b, $\nu_{CC(N)}$) to the SiO_2 support (HPy). This mode arises at slightly lower wavenumbers at 1445 cm^{-1}. The weak shoulder at ~1433 cm^{-1} on the band at 1447 cm^{-1} is assigned to physisorbed pyridine on the SiO_2 support (PPy). The broad feature at 1638 cm^{-1} corresponds to mode 8a ($\nu_{CC(N)}$) on Brønsted acid sites. The peak at 1607 cm^{-1} is tentatively assigned to mode 8a ($\nu_{CC(N)}$) of pyridine coordinated to Lewis acid sites [65]. As shown later, this band is retained up to 523 K and is thus strongly held on the Ni_2P surface. The features at 1595 and 1576 (or 1578) cm^{-1} likely correspond to 8a modes ($\nu_{CC(N)}$) of pyridine hydrogen-bonded to the SiO_2 support.

There are a number of modes for the hydrogen-bonded and physisorbed pyridine which do not appear as distinct bands. We surmise that this is because of overlap with similar bands for the closely related pyridine species on Brønsted and Lewis acid sites, and have so indicated this in Table 4.

The spectrum for pyridine adsorption on Ni_2P/SiO_2 in H_2 flow (Fig. 5) exhibits several important differences compared to the spectrum under He flow (Fig. 4). In the high wavenumber region, two new weak features centered at 2957 and 2874 cm^{-1} are now visible and correspond to aliphatic ν_{CH} modes [66]. This is indicative of the formation of hydrogenated products on the catalyst surface. In addition, the features located at 1607 and 1447 cm^{-1} due to coordination of pyridine with Lewis acid sites (LPy) are greatly attenuated in intensity. The combination band (BPy/LPy) centered at 1491 cm^{-1} is also lower in intensity. As a result the initial reaction of the adsorbed pyridinium species likely occurs on Lewis acid centers because coverage on these sites is lower under reactive conditions.

Under H_2 flow, a new peak not observed under He flow emerges at 1481 cm^{-1}. As shown later, this band is not present in the spectrum of piperidine (PIP) adsorbed on Ni_2P/SiO_2. This peak is tentatively assigned to a ν_{C-C} mode of a partially hydrogenated pyridine molecule, possibly 2,3,4,5-tetrahydropyridine (THP) (IUPAC name: 3,4,5,6-tetrahydropyridin-2-yl), in view of the aliphatic ν_{CH} modes. A similar imine species was previously reported by the group of Prins [52]. As will be shown shortly, this peak is not associated with the formation of piperidine on the catalyst surface.

In Fig. 6 for Ni_2P/SiO_2 in 0.85 mol% piperidine/He flow, two negative peaks at 3745 and 3669 cm^{-1} are again present due to interaction of piperidine with Si–OH and P–OH groups, respectively. A prominent shoulder on a rising background was also located at ~3265 cm^{-1} and is assigned to a ν_{NH} stretching mode of piperidine [66]. As expected, no contributions due to aromatic ν_{CH} modes are observed but several strong peaks corresponding to aliphatic ν_{CH} vibrations are observed at 2943, 2864, 2806 and 2739 cm^{-1}. In the low wavenumber region, a prominent broad band is located at 1620 cm^{-1}. A previous study on 2-methylpiperidine adsorption on Ni_2P/SiO_2 assigned this band to the NH_2 scissoring mode arising from the protonation of the piperidine nitrogen atom and formation of an adsorbed piperidinium intermediate. In addition, a medium intensity peak at 1474 cm^{-1} overlaps a strong band centered at 1458 cm^{-1}. Analogous to the results obtained for 2-methylpiperidine adsorption, these overlapping bands correspond to ν_{C-C} and ν_{C-N} stretching modes, respectively [13]. The features at 1620 and 1474 cm^{-1} exhibit similar intensity. Also, the peak at 1458 cm^{-1} has a prominent shoulder at ~1450 cm^{-1} likely due to piperidine hydrogen-bonded (HPip) to the SiO_2 support.

The effect of temperature on pyridine adsorbed on SiO_2 and Ni_2P/SiO_2 in both He and H_2 flow was examined to probe the relative stability of adsorbed pyridine and the nature of surface acid sites. As can be seen in Fig. 7, SiO_2 does not possess sites with Brønsted or Lewis character as no peaks attributable to a surface pyridinium species are present. Pyridine is only weakly hydrogen-bonded to the surface hydroxyl groups and little pyridine remains at 523 K. As stated earlier, no changes in the spectra were observed upon switching the carrier flow to H_2, indicating that SiO_2 is an innocent support, i.e. it does not hold reactive intermediates [67]. The absorbance features in Fig. 8 for pyridine adsorbed on Ni_2P/SiO_2 in He flow also exhibit a similar response to temperature. At temperatures above 373 K, the bands centered at 1638 and 1547 cm^{-1} due to pyridine bonded to Brønsted acid sites have been attenuated. Conversely, absorbance features attributable to pyridine coordinated to Lewis acid sites at 1607 and 1447 cm^{-1} are retained up to 523 K. These results indicate that Ni centers (Lewis sites) have stronger acidity than surface Brønsted acid sites.

The FTIR features in Fig. 9 for pyridine adsorbed on Ni_2P/SiO_2 in H_2 flow display similar responses to increasing temperature as those in Fig. 8. The features due to Brønsted-bonded pyridine were again rapidly diminished with heating. Under H_2 flow, the peaks attributable to pyridine coordinated to Lewis acid sites diminished more rapidly compared to the spectra in He flow. This is expected as hydrogenation of pyridine likely occurs on Lewis acid sites. At 473 K, features at 1481 and 1460 cm^{-1} are visible and become dominant compared to the band at 1491 cm^{-1}. These bands are observed to grow in intensity with further heating up to 523 K, indicating that they are reaction products. As discussed earlier, the peak at 1481 cm^{-1} can be tentatively assigned to the partially hydrogenated product 2,3,4,5-tetrahydropyridine. The peak at 1460 cm^{-1} can be assigned to the ν_{C-N} mode of piperidine.

4.3. Analysis of coverage transients

Although in situ characterization of Ni_2P catalysts has been carried out in the past [68–70], the ACT method relies on the measurement of in situ transient kinetic data and these will be described in this section. Transient experiments were performed on the Ni_2P/SiO_2 catalyst at 423 K using several concentrations of pyridine in both He and H_2 flow in order to distinguish between the net rates of adsorption and the rates of reaction. For all experiments, the evolution of the peak at 1491 cm^{-1} (pyridinium species on Brønsted and Lewis acid centers) was tracked over time. This peak, representing pyridine on Brønsted and Lewis acid sites, was chosen because it is well resolved from other spectral fea-

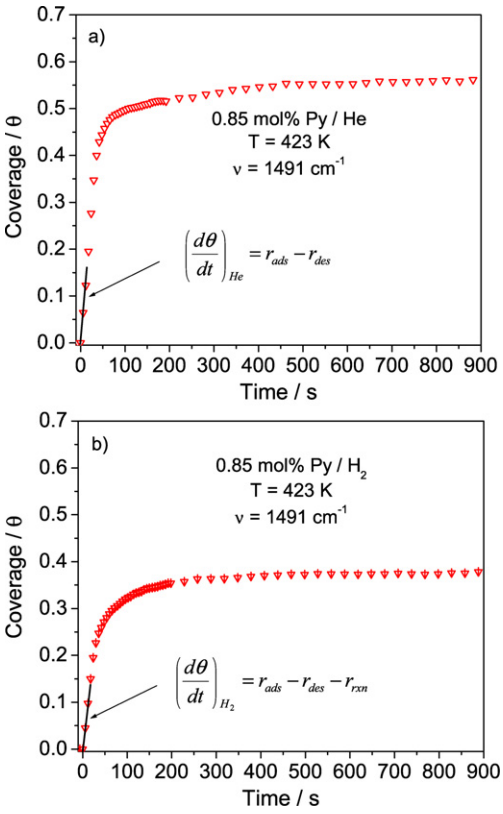

Fig. 12. Example of transient kinetic analysis for pyridine adsorption on Ni_2P/SiO_2. (a) He carrier at 423 K, (b) H_2 carrier at 423 K.

tures, is not present in the spectrum of gas-phase pyridine, and has no contribution from pyridine physisorbed on the active phase or SiO_2 support. Fig. 11 shows the evolution of the coverage (θ) of pyridine on acidic sites plotted as a function of time for various concentrations in He and H_2. Coverages are obtained by normalization of peak areas to the saturation peak area at room temperature as described in the experimental section. The adsorbed pyridinium species has the attributes of a reaction intermediate. Fig. 11 shows that its concentration goes up with pyridine partial pressure, goes down when the flow is switched from He to H_2, and Fig. 9 shows that its concentration goes down with reaction temperature.

Fig. 12 shows an example of how the transient curves can be analyzed. The figure presents the evolution of pyridine coverage with respect to time for the addition of 0.85 mol% pyridine in He or H_2 carrier at 423 K. As can be seen, pyridine was introduced to the reactor at time zero and the coverages of pyridine quickly increased to a steady value in ~200 s under both carrier gases. As a note, coverage values are shown in 6 s increments in the transient region of the coverage curve (<200 s) and at 30 s intervals thereafter. In He carrier (Fig. 12a), the coverage of pyridine reached a steady-state value of 0.56. As expected, because of the occurrence of reaction, the steady-state coverage of pyridine in H_2 carrier (Fig. 12b) was lower and reached a value of 0.38. At all concentrations used in the study, the steady-state coverage of pyridine on Ni_2P/SiO_2 was lower in reactive H_2 carrier than in inert He carrier gas because of reaction of pyridine.

Rates are determined by extrapolating the slope ($d\theta/dt$) in the transient region of the adsorption isotherms to time zero. The derivative represents a turnover frequency (TOF, s^{-1}). A way to understand this is to consider a surface that goes from full coverage to zero coverage in 1 s, which would correspond to a TOF of 1 s^{-1}. Fig. 12a shows the evolution of pyridine coverage as a function of time for pyridine adsorption (0.85 mol%) in He carrier at 423 K. The slope of the coverage versus time curve is equal to the

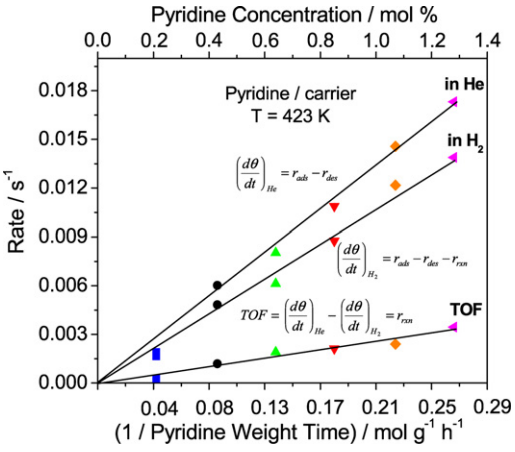

Fig. 13. Transient kinetic results for pyridine reaction on Ni_2P/SiO_2 at 423 K.

net rate of adsorption, that is, the rate of pyridine adsorption (r_{ads}) minus the rate of pyridine desorption (r_{des}):

$$\left(\frac{d\theta}{dt}\right)_{He} = r_{ads} - r_{des}. \quad (4)$$

The rate of adsorption is proportional to the number of empty sites and the rate of desorption is proportional to the number of occupied sites. As a result, the rate of adsorption decreases with increasing coverage while the rate of desorption increases. At steady-state these rates are equilibrated and the apparent net rate of adsorption is zero. Fig. 12b shows the analogous method used for pyridine adsorption (0.85 mol%) in H_2 carrier at 423 K. The slope of the coverage versus time curve now represents the rate of pyridine adsorption (r_{ads}) minus the rate of pyridine desorption (r_{des}) minus the rate of pyridine reaction (r_{rxn}):

$$\left(\frac{d\theta}{dt}\right)_{H_2} = r_{ads} - r_{des} - r_{rxn}. \quad (5)$$

For each pyridine weight time, the rate of surface reaction is determined by subtraction of the independently determined rates:

$$\left(\frac{d\theta}{dt}\right)_{He} - \left(\frac{d\theta}{dt}\right)_{H_2} = r_{rxn}. \quad (6)$$

The measured rates are compared with the overall turnover frequency of pyridine determined in a separate experiment.

Fig. 13 presents the results of the analysis just described for the rates measured in He and H_2 and their differences, the turnover frequencies of the adsorbed pyridine species. As shown, the measured rates in both He and H_2 carriers increased linearly with increasing pyridine concentration and decreasing weight time. Moreover, the rates measured in H_2 carrier were lower at all concentrations and weight times, as discussed previously. As the pyridine concentration was increased the differences between the rates measured independently in He and H_2 also increased, giving rise to a steadily increasing reaction rate of pyridine. The turnover frequency trend was linear with increasing pyridine concentration, indicating a first-order reaction. However, over the range of concentrations studied the rates of pyridine reaction were low.

Fig. 14 shows the steady-state pyridine turnover frequencies measured in a similar range of pyridine weight time as used in the transient experiments. These TOFs were calculated from Eq. (3) and are based on sites counted by the chemisorption of CO. There is no sulfur in the feed, so there is no phosphosulfide [14,29,69,71], and the uptakes are reasonable measures of surface atoms [28,72]. The pyridine saturation coverage is similar. As can be seen, the overall turnover frequency of pyridine increased linearly with decreasing weight time. Although displaying the same trend, the

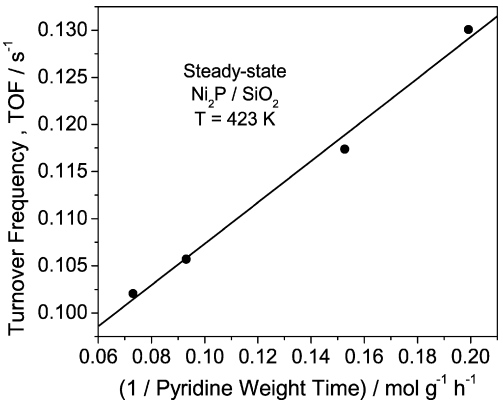

Fig. 14. Steady-state kinetic results for pyridine reaction over Ni_2P/SiO_2 at 423 K and atmospheric pressure.

rates measured under steady-state conditions were observed to be two orders of magnitude higher than those measured under transient conditions. It is recognized that the transient rates are obtained by extrapolation to zero coverage, but for this reason these rates are maximal, and yet are smaller than the steady-state rates. Initial steady-state rates cannot be measured with our unit, but are expected to start out low and reach a plateau, as is observed with standard hydroprocessing catalysts [29,30,75]. It is concluded that the main species observed under reaction conditions, the pyridinium species on Brønsted and Lewis acid sites, is not the reactive intermediate in the reaction but a spectator that reacts at a much lower rate that the overall rate of reaction (Scheme 1).

The question arises whether another species could be a reactive intermediate. A possible candidate is the partially hydrogenated species with characteristic band at 1481 cm^{-1} and aliphatic ν_{CH} bands at 2957 and 2874 cm^{-1}. The species was not observed under He flow but was formed upon adsorption of pyridine on Ni_2P in reactive H_2. It is an imine, the species identified by Prins and coworkers as a possible reaction intermediate [43,44]. Unfortunately, the same analysis as done for the pyridinium ion cannot be carried out with this species because it is not observed in experiments conducted under He flow. However, we conjecture that it is a reactive intermediate (Scheme 1).

Hydrogenation of pyridine likely occurs on Lewis acid sites as reaction of pyridine and formation of the partially hydrogenated intermediate results in attenuation of the peaks located at 1607, 1491 and 1447 cm^{-1}. This is in agreement with the work of Miranda and coworkers [73] who studied the HDN of pyridine at atmospheric pressure over several supported Mo oxides with varying Lewis and Brønsted acidities. They determined that the overall HDN activity was correlated with the concentration of cus Mo sites which are active for hydrogenation, and reaction of pyridine to piperidine was rate-limiting.

One possible explanation for the slow conversion of the pyridinium species and the formation of a partially hydrogenated surface intermediate is the mode of pyridine adsorption under the reaction conditions employed. Pyridine can adsorb on the catalyst surface via the nitrogen atom's electron pair (end-on mode) or through the π electrons of the aromatic ring (side-on mode) [36]. It has been proposed that ring hydrogenation occurs through side-on adsorption while C–N bond cleavage takes place through the end-on mode [74]. Green and coworkers [75,76] studied the HDN of pyridine over transition metal carbides, oxides, nitrides and sulfides over a wide temperature range and determined from product distributions and selectivities that the end-on mode is favorable at low temperatures while the side-on adsorption mode is favorable at higher temperatures.

From our results, it can be suggested that at the low reaction temperature (423 K) the observed pyridinium species corresponds to pyridine adsorbed in the end-on mode. As a result, further reaction of adsorbed pyridine in this mode is extremely slow and the species is only a spectator in the overall HDN reaction. Adkins and coworkers studied the hydrogenation of pyridine and 2,6-dimethylpyridine over Raney nickel and observed a higher hydrogenation rate for 2,6-dimethylpyridine. The observations were ascribed to a steric effect by which 2,6-dimethylpyridine was adsorbed to the catalyst surface via a surface π-complex. The unhindered pyridine molecule was assumed to adsorb through the sp^2 lone electron pair in the end-on mode. The side-on adsorption was proposed to be favorable for hydrogenation [77]. It is important to note that, under our experimental conditions, $P_{H_2} = 1$ atm and $T = 423$ K, the hydrogenation reaction of pyridine to piperidine is not limited by thermodynamics. The thermodynamic equilibrium equation [78] indicates that equilibrium lies well to the right:

$$\ln K = \frac{23470}{T} - 46.06 + 3\ln\left(\frac{P_{H_2}}{P^o}\right), \tag{7}$$

where $K = [\text{piperidine}]/[\text{pyridine}]$, T [=] K and $P^o = 1$ atm. The value of K is 1.24×10^4. Thus, the pyridine–piperidine equilibrium is completely on the piperidine side.

The true reaction intermediate likely arises via pyridine adsorbed in the side-on arrangement, as this mode is more favorable for hydrogenation of the aromatic ring. Analogous to the hydrogenation of aromatics on metals, it is generally believed that hydrogenation of nitrogen heterocycles proceeds with the ring parallel to the surface via formation of a surface π-adsorbed intermediate. Electrons in d-orbitals of the Ni atoms are available for π-back bonding into the empty antibonding π-molecular orbitals of pyridine, thus destroying the aromaticity of the molecule and activating it for hydrogenation [79]. The appearance of a partially hydrogenated species on the Ni_2P surface instead of the fully saturated intermediate piperidine is understandable since hydrogenation reactions of aromatics are know to be slow at low temperatures and H_2 pressures [80]. Furthermore, accumulation of the partially hydrogenated intermediate on the catalyst surface can be explained by strong adsorption and the absence of H_2S in the feed. The partially saturated and fully saturated intermediates formed after hydrogenation are more strongly basic than the unsaturated reactant [81]. As a result, they are strongly held on the surface of the Ni_2P catalyst. The absence of H_2S in the feed, which is known to promote ring-opening by addition to the C=N bond [43] or by a classic organic mechanism [82], probably diminishes further reaction of the adsorbed intermediate.

To summarize, an adsorbed pyridinium species was identified on the surface of Ni_2P/SiO_2 at reaction conditions. The species behaved as a reactive intermediate, as its concentration increased with increasing pyridine partial pressure and decreased with exposure to hydrogen. However, a study of the kinetics of its reaction using transient experiments showed that it reacted at a rate about 100 times slower than the steady-state reaction. This indicated that it was not a true reaction intermediate, but a spectator on the surface. The studies here demonstrate the danger of carrying out spectroscopic measurements of surface species without doing dynamic experiments to verify that they are capable of reacting at rates consistent with catalytic rates.

5. Conclusions

A method for studying reaction mechanisms, denoted as analysis of coverage transients (ACT), is described which allows determining whether an observed surface species is an actual reaction intermediate. The ACT method compares the response in time of

the surface species in inert and reactive atmospheres and compares this to the steady-state reaction rate. A match between the rate of reaction determined in the transient experiments with that of the reaction turnover frequency (TOF) indicates that the species is a reactive intermediate [3], while a mismatch points to the species being a spectator on the surface.

The method is applied to the hydrodenitrogenation (HDN) of pyridine over Ni_2P/SiO_2 at 423 K and atmospheric pressure. FTIR experiments were used to identify a pyridinium intermediate with characteristic bands at 1607, 1491 and 1446 cm^{-1} on the Ni_2P surface under He flow. Upon switching the carrier flow to H_2, a second band at 1481 cm^{-1} was identified and assigned to a partially hydrogenated reaction intermediate. Transient kinetic experiments, conducted under both He and H_2 flow, were used to separately measure the net rate of adsorption and the rate of reaction of the pyridinium species. Comparison to the steady-state turnover frequency at the same reaction conditions showed that the TOF was two orders of magnitude higher than the reaction rate obtained under transient conditions. The mismatch indicated that the pyridinium species is a spectator in the HDN of pyridine. Under the reaction conditions employed, pyridine is likely adsorbed to the catalyst surface through the nitrogen atom lone pair (end-on mode) through which hydrogenation is slow. The partially hydrogenated species, the imine 2,3,4,5-tetrahydropyridine, observed under H_2 flow is a possible reaction intermediate in the HDN of pyridine.

Acknowledgment

This work was supported by the US Department of Energy, Office of Basic Energy Sciences, through Grant DE-FG02-963414669.

References

[1] S.T. Oyama, W. Li, Top. Catal. 8 (1999) 75.
[2] J.J. Bravo-Suárez, K.K. Bando, J.Q. Lu, M. Haruta, T. Fujitani, S.T. Oyama, J. Phys. Chem. C 112 (2008) 1115.
[3] J.J. Bravo-Suárez, K.K. Bando, T. Fujitani, S.T. Oyama, J. Catal. 257 (2008) 32.
[4] K. Tamaru, Trans. Faraday Soc. 57 (1961) 1410.
[5] K. Tamaru, Dynamic Heterogeneous Catalysis, Academic Press, London, 1978.
[6] K. Tamaru, in: G. Ertl, H. Knözinger, J. Weitkamp (Eds.), Handbook of Heterogeneous Catalysis, vol. 3, VCH, Weinheim, 1997, p. 1013.
[7] W.R.A.M. Robinson, J.N.M. van Gastel, T.I. Korányi, S. Eijsbouts, J.A.R. van Veen, V.H.J. de Beer, J. Catal. 161 (1996) 539.
[8] W. Li, B. Dhandapani, S.T. Oyama, Chem. Lett. (1988) 207.
[9] C. Stinner, R. Prins, Th. Weber, J. Catal. 202 (2001) 187.
[10] V. Zuzaniuk, R. Prins, J. Catal. 219 (2003) 85.
[11] S.T. Oyama, J. Catal. 216 (2003) 343.
[12] S.T. Oyama, Y.-K. Lee, J. Phys. Chem. B 109 (2005) 2109.
[13] Y.-K. Lee, S.T. Oyama, J. Catal. 239 (2006) 376.
[14] S.T. Oyama, Y.-K. Lee, J. Catal. 258 (2008) 393.
[15] H. Topsøe, B.S. Clausen, F.E. Massoth, Hydrotreating Catalysis—Science and Technology, Springer-Verlag, Berlin, 1996.
[16] J.M. Thomas, W.J. Thomas, Principles and Practice of Heterogeneous Catalysis, VCH, New York, 1997.
[17] C. Song, Catal. Today 86 (2003) 211.
[18] S.T. Oyama, T. Gott, H. Zhao, Catal. Today (2009), doi:10.1016/j.cattod.2008.09.019.
[19] S.E. Eisjbouts, J.A.R. van Veen, E.J.M. Hensen, G. Mul (Eds.), Fourth International Symposium on Molecular Aspects of Catalysis by Sulfides, Doorn, The Netherlands, May 13–17, 2007, Catal. Today 130 (2008).
[20] J.R. Katzer, R. Sivasubramanian, Catal. Rev. Sci. Eng. 20 (2) (1979) 155.
[21] P. Grange, Catal. Rev. Sci. Eng. 21 (1) (1980) 135.
[22] F. van Looij, P. van der Laan, W.H.J. Stork, D.J. DiCamillo, J. Swain, Appl. Catal. A 170 (1998) 1.
[23] S. Shin, H. Yang, K. Sakanishi, I. Mochida, D.A. Grudoski, J.H. Shinn, Appl. Catal. A 205 (2001) 101.
[24] G.C. Laredo, E. Altamirano, J.A. De los Reyes, Appl. Catal. A 243 (2003) 207.
[25] P. Zeuthen, K.G. Knudsen, D.D. Whitehurst, Catal. Today 65 (2001) 307.
[26] U.T. Turaga, X. Ma, C. Song, Catal. Today 86 (2003) 265.
[27] A. Logadóttir, P.G. Moses, B. Hinnemann, N.-Y. Topsøe, K.G. Knudsen, H. Topsøe, J.K. Nørskov, Catal. Today 111 (2006) 44.
[28] X. Wang, P. Clark, S.T. Oyama, J. Catal. 208 (2002) 321.
[29] S.T. Oyama, X. Wang, Y.-K. Lee, K. Bando, F.G. Requejo, J. Catal. 210 (2002) 207.
[30] S.T. Oyama, X. Wang, Y.-K. Lee, W.-J. Chun, J. Catal. 221 (2004) 263.
[31] C.L. Yaws, K.P. Narasimhan, C. Gabbula, Yaws' Handbook of Antoine Coefficients for Vapor Pressure, Knovel, 2005.
[32] S. Rundqvist, Acta Chem. Scand. 16 (1962) 992.
[33] Powder Diffraction Data Files, JCPDS International Center for Diffraction Data, Swathmore, PA, 1992.
[34] N. Nelson, R.B. Levy, J. Catal. 58 (1979) 485.
[35] G. Perot, Catal. Today 10 (1991) 447.
[36] M.J. Ledoux, P.E. Puges, G. Maire, J. Catal. 76 (1982) 285.
[37] J. Sonnemans, W.J. Neyens, P. Mars, J. Catal. 34 (1974) 230.
[38] J. Sonnemans, P. Mars, J. Catal. 34 (1974) 215.
[39] R. Prins, M. Jian, M. Flechsenhar, Polyhedron 16 (1997) 3235.
[40] M. Jian, R. Prins, J. Catal. 179 (1998) 18.
[41] I.I. Abu, K.J. Smith, Catal. Today 125 (2007) 248.
[42] I.I. Abu, K.J. Smith, Appl. Catal. A 328 (2007) 58.
[43] H. Wang, C. Liang, R. Prins, J. Catal. 251 (2007) 295.
[44] M. Egorova, Y. Zhao, P. Kukula, R. Prins, J. Catal. 206 (2002) 263.
[45] J.F. Cocchetto, C.N. Satterfield, Ind. Eng. Chem. Process Des. Dev. 15 (1976) 272.
[46] J.F. Cocchetto, C.N. Satterfield, Ind. Eng. Chem. Process Des. Dev. 20 (1981) 49.
[47] G.C. Hadjiloizou, J.B. Butt, J.S. Dranoff, J. Catal. 131 (1991) 545.
[48] P. Clark, X. Wang, P. Deck, S.T. Oyama, J. Catal. 210 (2002) 116.
[49] M. Cattenot, J.-L. Portefaix, J. Afonso, M. Breysse, M. Lacroix, G. Perot, J. Catal. 173 (1998) 366.
[50] Y. Zhao, R. Prins, J. Catal. 222 (2004) 532.
[51] Y. Zhao, P. Kukula, R. Prins, J. Catal. 221 (2004) 441.
[52] R. Prins, Y. Zhao, N. Sivasankar, P. Kukula, J. Catal. 234 (2005) 509.
[53] A. Platon, W.J. Thomson, Ind. Eng. Chem. Res. 42 (2003) 5988.
[54] S. Damyanova, M.A. Centeno, L. Petrov, P. Grange, Spectrochim. Acta Part A 57 (2001) 2495.
[55] M.S. Rana, M.L. Huidobro, J. Ancheyta, M.T. Gómez, Catal. Today 107–108 (2005) 346.
[56] F. Sánchez-Minero, J. Ramírez, A. Gutiérrez-Alejandre, C. Fernández-Vargas, P. Torres-Mancera, R. Cuevas-Garcia, Catal. Today 133–135 (2008) 267.
[57] E.C. DeCanio, J.G. Weissman, Colloids Surf. A 105 (1995) 123.
[58] T.I. Korányi, M. Dobrovolszky, T. Koltai, K. Matusek, Z. Paál, P. Tétényi, Fuel Process. Technol. 61 (1999) 55.
[59] R.M. Navarro, P. Castaño, M.C. Álvarez-Galván, B. Pawelec, Catal. Today (2008), in press.
[60] Y.-C. Park, E.-S. Oh, H.-K. Rhee, Ind. Eng. Chem. Res. 36 (1997) 5083.
[61] K.A. Layman, M.E. Bussell, J. Phys. Chem. B 108 (2004) 10930.
[62] K.A. Layman, M.E. Bussell, J. Phys. Chem. B 108 (2004) 15791.
[63] M.I. Zaki, M.A. Hasan, F.A. Al-Sagheer, L. Pasupulety, Colloids Surf. A 190 (2001) 261.
[64] A.P. Legrand, H. Hommel, A. Tuel, Adv. Colloid Interface Sci. 33 (1990) 91.
[65] C. Morterra, G. Cerrato, Langmuir 6 (1990) 1810.
[66] G. Socrates, Infrared Characteristic Group Frequencies, Wiley, New York, 1994.
[67] M. Seman, J.N. Kondo, K. Domen, R. Radhakrishnan, S.T. Oyama, J. Phys. Chem. B 106 (2002) 12965.
[68] S.T. Oyama, X. Wang, F. Requejo, T. Sato, Y. Yoshimura, J. Catal. 209 (2002) 1.
[69] T. Kawai, K.K. Bando, Y.-K. Lee, S.T. Oyama, W.-J. Chun, K. Asakura, J. Catal. 241 (2006) 20.
[70] T. Kawai, W.J. Chun, K. Asakura, Y. Koike, M. Nomura, K.K. Bando, S.T. Oyama, H. Sumiya, Rev. Sci. Instrum. 79 (2008), 014101-1.
[71] A.E. Nelson, M. Sun, A.S.M. Junaid, J. Catal. 241 (2006) 180.
[72] S.T. Oyama, P. Clark, V.L.S. Teixeira da Silva, E.J. Lede, F.G. Requejo, J. Phys. Chem. B 105 (2001) 4961.
[73] J.A. Marzari, S. Rajagopal, R. Miranda, J. Catal. 156 (1995) 255.
[74] C. Moreau, P. Geneste, in: J.B. Moffat (Ed.), Theoretical Aspects of Heterogeneous Catalysis, in: Van Nostrand Reinhold Catalysis Series, 1990, p. 256.
[75] H.A. Al-Megren, T. Xiao, S.L. Gonzalez-Cortes, S.H. Al-Knowaiter, M.L.H. Green, J. Mol. Catal. A Chem. 225 (2005) 143.
[76] H.A. Al-Megren, S.L. González-Cortés, T. Xiao, M.L.H. Green, Appl. Catal. A 329 (2007) 36.
[77] H. Adkins, L.F. Kuick, M. Farlow, B. Wojcik, J. Am. Chem. Soc. 56 (1934) 2425.
[78] W.V. Steele, R.D. Chirico, Topical Report for the US Department of Energy, IIT Research Institute, Barstlesville, OK, 1992.
[79] T.C. Ho, Catal. Rev. Sci. Eng. 30 (1) (1988) 117.
[80] G.M. Loudon, Organic Chemistry, 3rd edition, Benjamin–Cummings, Redwood City, 1995, p. 775.
[81] M.-H. Yang, P. Grange, B. Delmon, Appl. Catal. A 154 (1997) L7–L15.
[82] E. Furimsky, F.E. Massoth, Catal. Rev. Sci. Eng. 47 (3) (2005) 297.